The 20th International Conference on
Transport and Sedimentation of Solid Particles
26–29th September 2023, Wroclaw, Poland

ISSN 0867-7964 ISBN 978-83-7717-392-3

EFFECTS OF HEAVE MOTION ON THE DYNAMIC RESPONSE OF THE BLOCKED HYDRAULIC LIFTING SYSTEM

Huade Cao[1,2], Qiang Yang[1,2], Jianxin Xia[1,2,*], Xinyu Zhang[1,2]

DOI: 10.30825/4.14-22.2023

1.China University of Geosciences (Beijing), Beijing, China, 100083
2. Key Laboratory of Polar Geology and Marine Mineral Resources（China University of Geosciences, Beijing）, Ministry of Education, Beijing, China, 100083
**Corresponding author. E-mail: jxxia@vip.sina.com*

ABSTRACT: Growing economy causes the shortage of mineral resource in the near future. The mineral resource locates at the sea bottom floor is an alternative solution. The hydraulic lifting technique is the priority option for the deep-sea mining. However, the heave motion caused by ocean wave leads to longitudinal vibration of the lifting pipe, which is also influenced by fluid structural interaction effect between the internal fluid and the pipe wall. During the longitudinal vibration, the closed end due to blockage or malfunction of the buffer will either pull or push the internal fluid that activates the pressure wave oscillation. The partitioned shell-based water hammer model is advanced to replicate the longitudinal vibration of the fluid-filled lifting pipe with one end closed. For parametric study, the frequency of the heave motion varies in the frequency range of the natural ocean wave. The masses of the lifting pump and buffer are treated as concentrated masses. Effects of concentrated masses, length of lifting pipe on the pipe dynamic response are investigated. Three resonant frequencies in the investigated range for the full scale of ocean mining lifting system are found. The first and the third resonance frequencies are identical to the frequencies of the water hammer pressure wave and the stress wave oscillation, respectively. The second resonant results from the coupling between the water hammer pressure wave and the stress wave. It also found that there is always an excited frequency a bit over the resonance frequency which depresses dynamic response of the fluid-filled lifting pipe.

KEY WORDS: Deep-sea mining, heave motion, longitudinal vibration, partitioned water hammer model, resonance.

1. INTRODUCTION

The deep-minerals attracts more attention in recently, as it is an alternative option to solve the mineral shortages alongside with the rising of world population and economic (Heffernan, 2019). On the sea floor over a depth of 4000m, the well-known Clarion-Clipperton Zone (CCZ) reserves trillions of potato-sized polymetallic nodules and holds more of certain metals than land deposits. These metals could satisfy the growing demand for the green technology to achieve a sustainable development goal, such as batteries to

store wind, solar and ocean wave energy and power electric cars. In fact, the deep-sea mining technology to extract the polymetallic nodules from the deep-sea has a long history, more than 50 years (Sparenberg, 2019). Mechanical lifting and hydraulic lifting have been investigated for the transportation of the polymetallic from the sea floor to sea surface (Verichev et al., 2011). Since the hydraulic lifting can provide continuous productions, it is more efficient than the mechanical lifting.

The hydraulic lifting system for deep sea mining is depicted in Figure 1, which consists of seabed mining vehicles, flexible riser, buffer, lifting pump and rising pipe, as well as mining vessel and shipping vehicle on the sea surface. The waster water along with the nodules of hydraulic transportation is discharged back under the sea surface with a depth of 1000m to decease the environment impact (Heffernan, 2019). Under the harsh ocean environment, the lifting system consisting of a buffer, lifting pump and pipe is vulnerable which can be simplified as a fluid-filled hanging pipe with concentrated masses.

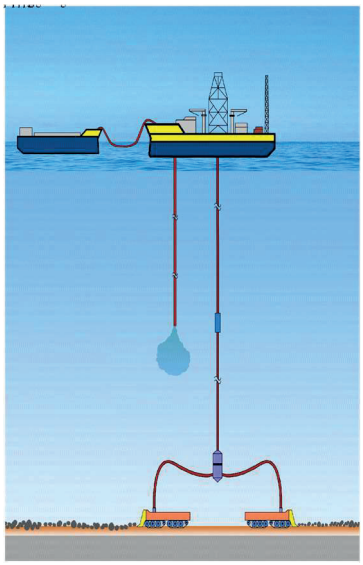

Figure 1 Deepsea mining system

The internal fluid is a key factor for the stability of the lifting pipe system. Based on theoretical analysis, Paidoussis (1970) found that both the hanging pipe and standing pipe lose stability by flutter after a critical high flow velocity. In the case of a hanging pipe aspirating fluid, the fluid flows from the free end to the fixed end that consistent with the flow direction in the lifting system for ocean mining. Paidoussis and Luu (1985) found that aspirating pipe loses stability at extremely low speed, which is contradicted to the experimental observation. Paidoussis (1999) attributed this contradiction to the absence of negative pressurisation in the theoretical equations. Based on theoretical analysis, Kuiper and Metrikine (2005) attributed this contradiction to the hydrodynamic drag caused by surrounding water. In further work, Kuiper and Metrikine (2008) experimentally observed

the cantilever aspiring pipe lose stability beyond a critical velocity of the inner flow. Using experimental, numerical and analytical methods to investigate cantilevered aspirating pipes, Giacobbi et.al., (2012) observed first-mode flutter as the inner flow beyond the critical velocity. Unlike a cantilever pipe with a fixed end, Chatjigeorgiou (2010) accounted for the top excitations in aspiring pipe with plug flow and found that the effect of the axial force due to inner steady flow is negligible for the lifting pipe dynamic response. Considering the density variation in the inner flow, Bai et.al., (2018) improved the stability criterion of the lifting pipe stability for ocean mining. Aforementioned published works on the inner flow are focus on the steady flow. Few literatures investigate the dynamic response due to unsteady flow (water hammer) caused by blockage or malfunction of pump and valve in ocean mining.

There are a lot of work on water hammer, accounting for the fluid-structural interaction effect in fluid-filled pipe. Skalak (1953) predicted a precursor pressure wave travelling with the speed close to the sound speed in the pipe wall, which was experimentally observed by Williams (1977). Based on experimental observations, Budny et.al., (1990, 1991) investigated the effects of structural damping on the dynamic response of fluid and structural fields during water hammer. Tijsseling and Lavooij (1990) classified the fluid-structural interaction effects into friction, Poisson and junction coupling. Water hammer accounting for the fluid-structural interaction effects were experimentally investigated in the L-shape (Tijsseling & Vaugrante, 2001) and T-shape pipes (Vardy et al., 1996). Various numerical methods have been adopted to solve the water hammer accounting for the fluid structural interaction effects, e.g., the method of characteristics (Wiggert & Sundquist, 1997; Wiggert & Tijsseling, 2001), the Godunov's method (Daude & Galon, 2018; Gale & Tiselj, 2008). To remedy the limitations of the monolithic water hammer models, Cao et.al. (2021) proposed a partitioned water hammer model accounting for the fluid structural interaction, which adopted an axisymmetric finite element based on thin-shell theory (Cao et al., 2020). The boundary conditions investigated in the published works are either fixed or longitudinal free. However, the top boundary of the lifting pipe is forced to oscillate that needs further investigation for the water hammer phenomenon accounting for fluid-structural interaction.

According to the above brief review, the published works interested on the longitudinal vibration due to heave motion do not account for the internal unsteady flow, and those works interested on the unsteady flow do not account for the forced boundary condition. Hence, the present work focus on the water hammer in a lifting pipe, accounting for the forced boundary due to the heave motion of the surface vessel. Accounting for the concentrated masses of pump and buffer in the finite element model, the dynamic response is obtained for lifting pipe subjected to heave motion. Using the partitioned algorithm, the finite element is adopted in conjunction with a fluid model for a fluid-filled lifting pipe with one end closed. The proposed partitioned water hammer model is solved to obtain the dynamic response of fluid-filled rising pipe with one end closed. Effects of the pipe length and masses of the pump and buffer, as well as the frequency of heave motion on the dynamic response of the rising pipe, are investigated both in an empty and fluid-filled pipe. The manuscript also investigates the effects of the initial internal flow velocity on the dynamic response of fluid-filled lifting pipe.

2. STATEMENT OF THE PROBLEM

Neglecting effects of surrounding water and the influence of flexible riser, the schematic of hydraulic lifting system in ocean mining system (Figure 1) is depicted in Figure 2. The heave motion of the mining vessel is simplified as a forced sinusoidal heave motion applied at the top of the lifting pipe. The origin O of cylindrical coordinate (z,r) locates at the centre of the pipe cross-section at sea surface. The axis z is oriented along the pipe axis and the axis r is oriented along the radial direction. The lifting pipe has a length of L with a length of L_1 for section OP and a length of L_2 for section PB, i.e., $L = L_1 + L_2$. The steel lifting pipe has a uniform circular cross-section with mid-surface radius R and thickness h. The steel has Young's modulus E, the Poisson's ratio ν and a density of ρ_s. The internal water has a density of ρ_f and bulk modulus of K_f. The buffer with mass M_b locates at the bottom of the lifting pipe and a pump with mass M_p locates at the intermediate of the lifting pipe. The initial velocity of in viscid inner flow is V_0, negative value for fluid flow from sea floor to sea surface. Due to the heave motion of the mining vessel, the top of the pipe is forced to oscillate sinusoidally with a displacement $u_{top} = A_e \sin(w_e t)$, in which A_e is the amplitude and w_e is the frequency of the excited sinusoidal wave. Due to the blockage or malfunction at the bottom of the lifting pipe, water hammer wave oscillates in the pipe and couples to the forced oscillation of the lifting pipe. It's required to investigate the influence of the vertical oscillation of the pipe top on the wave hammer phenomenon.

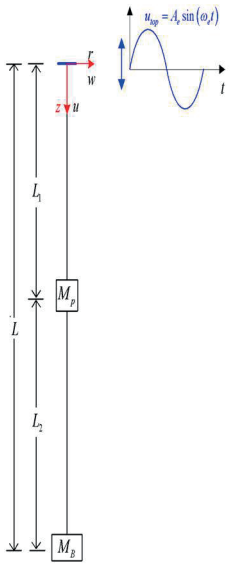

Figure 2 Schematic of the hydraulic lifting pipe system subjected to sinusoidal heave motion

3. PARTITIONED SHELL-BASED WATER HAMMER MODEL

Based on the assumption for the pipe dynamic response, mostly water hammer models can be classified into the classical water hammer models, which neglects the coupling effects between the pipe dynamic response and the transient flow (Ghidaoui et al., 2005), and the extended water hammer models (Tijsseling, 1996; Tijsseling et al., 2008), which accounting for the coupling effects between the transient flow and the longitudinal dynamic response of the pipe. The classical and extended water hammer models are commonly solved using the monolithic scheme, in which, both the fluid and the structural governing equations are solved simultaneously in each time step (Lavooij & Tijsseling, 1991; Tijsseling & Lavooij, 1990). In contrast, the partitioned water hammer models are enhanced in the modularity and robust in handling complex scenarios as illustrated in Cao et.al., (2021). Hence, the partitioned shell-based water hammer model from Cao et.al., (2021) is adopted and advanced in present work to handle the forced oscillation boundary at the top of the lifting pipe. For self-contained and avoid repetition, the partitioned shell-based water hammer model is simply summarized in this section.

In the partitioned water hammer models, the one-dimensional mass and momentum conservation equations for the inviscid fluid have been developed to capture the transient sectional pressure $P(x,t)$ and velocity $V(x,t)$ field in the fluid domain, given as

$$\frac{\partial V}{\partial z}+\frac{1}{K_f}\frac{\partial P}{\partial t}+\frac{2}{R-0.5h}\frac{\partial w}{\partial t}=0 \quad (1)$$

$$\frac{\partial V}{\partial t}+\frac{1}{\rho_f}\frac{\partial P}{\partial z}+g\sin\alpha=0 \quad (2)$$

where $w=w(z,t)$ is the radial displacement of inner surface of pipe, g is the gravity acceleration, t denotes time, α is the angle between pipe and horizontal direction, e.g., $\alpha=0$ for a horizontal pipe and $\alpha=90^{\circ}$ for a vertical pipe. Using the method of characteristics, Equations (1) and (2) are transferred into two ordinary differential equations along the positive and negative characteristic lines. The incline of the characteristic lines in the fluid model is equivalent to the sound speed in the fluid, i.e., $a_f=\sqrt{K_f/\rho_f}$. The actual water hammer wave speed a_w is lower than the sound speed a_f due to fluid-pipe interaction effects.

The values of the radial displacement $w(z,t)$ are obtained from the axisymmetric shell-based structural model, given as

$$\mathbf{M}\ddot{\mathbf{U}}(t)+\mathbf{C}\dot{\mathbf{U}}(t)+\mathbf{K}\mathbf{U}(t)=\mathbf{F}(t) \quad (3)$$

where M is the mass matrix, K is the stiffness matrix and C is the Rayleigh damping matrix, the nodal displacement vector $U^T(t)=\langle u_1\ w_1\ w_1'\ u_2\ w_2\ w_2'\rangle$ consists of the longitudinal displacement u_1, the radial displacement w_i and the rotation of the pipe wall w_i' due to the curvature of the radial displacement, subscript i denotes the first node and the second node of the axisymmetric shell-based element, and $F(t)$ is the energy equivalent load vector resulting from the water hammer pressure $P(z,t)$ loaded on the pipe inner surface. The first radial predominant and the first longitudinal

predominant modes are chosen to determine the Rayleigh damping matrix. The constant-average-acceleration method is adopted for the time integration. Unlike the structural model adopted in the classical and extended water hammer model, the shell-based structural model accounts for the radial inertial effects, as well as the gradient and curvature of the radial displacement around the wave front and boundaries. The model also offers flexibility in modeling various types of radial, longitudinal and rotational boundary conditions. This is the main reason to adopt the shell-based partitioned water hammer model for the water hammer problem in rising pipe for ocean mining impacted by the heave motion.

Using the partitioned scheme, the fluid model and the structural model are solved sequentially and iterated until specified convergence obtained in each time step.

4. REFERENCE CASE

A rising pipe is considered without the effects of surrounded water and the flexible riser. The inner water is considered as in viscid fluid. The length of section OP is $L_1 = 200m$ and $L_2 = 800m$ for section PB. The mid-surface of pipe is $R = 0.2m$ with a thickness of $h = 15mm$. Pipe material density is $\rho_s = 7800kg/m^3$ with the Young modulus of $E = 210GPa$ and a Poisson's ratio of $v = 0.25$. The internal flow has a density of $\rho_f = 1000kg/m^3$ with a bulk modulus of $K_f = 2.1GPa$. The lifting pump has a mass of $M_p = 7500kg$ and the buffer has a mass of $M_b = 3000kg$. The initial velocity of the internal flow is $V(z,0) = 0$. Since the present work is only interested in the dynamic response of the lifting pipe, the gravity force and the static hydraulic pressure along the longitudinal axis due to gravity are ignored.

The boundary condition at the top is $H_{res} = 0$ for the fluid model and $w(z = 0) = w'(z = 0) = 0$ for the structural model. The excited heave motion at the top of the lifting pipe is $u_e = A_e sin\omega_e t$, in which $A_e = 1$ is adopted for all cases, the excited frequency is investigated in the range of $w_e \sim (0.2rad/s]$ that close to the frequency of ocean wave. At the pump and buffer, the boundary conditions are $w(z = L_1) = w'(z = L_1) = 0$ and $w(z = 0) = w'(z = L) = 0$ for the structural model. Without column separation at the bottom of the lifting pipe, the fluid velocity is identical to the longitudinal velocity of the closed end, i.e., $V(z = L) = \dot{u}(z = L)$ where the dot denotes derivative with respect to time. Based on the natural frequency analysis, the first radial predominant frequency is $w_r = 1.57rad/s$ and the first longitudinal predominant frequency is $\omega_l = 24082.6rad/s$. The damping ratio for the chosen modes to determine the Rayleigh damping matrix are set as $\xi_r = \xi_l = 5\%$. In order to obtain steady state response, a long simulation time $T = 1000s$ is simulated. Based on mesh sensitive analysis, the element length is fixed as $\Delta L = 1m$ Considering the efficiency and accuracy, the Courant number adopt an integer value $C_r = 10$ to determine time step as $\triangle t = Cr \triangle \frac{L}{a_f} = 69ms$.

5. LIFTING SYSTEM SUBJECTED TO HEAVE MOTION

5.1 DYNAMIC RESPONSE OF FLUID-FILLED LIFTING PIPE SUBJECTED TO HEAVE MOTION

The present partitioned shell-based water hammer model is used to simulate the water hammer phenomenon in the reference case. For the iterative process between the structural model and the fluid model in each time step, the matched interface is adopted for the data transfer and the Aitken technique is adopted to accelerate the iterative process. Using the structural model for the empty lifting pipe, the displacement, velocity and acceleration field at 1000s are adopted as the initial conditions for the fluid-filled lifting pipe system.

The histories of the displacement of the buffer are plotted in Figure 10(a) with excited frequency $\omega_e = 1.08rad/s$ and in Figure 10(b) with excited frequency $\omega_e = 1.22rad/s$. Figure 10 (a) and (b) show that steady state response is obtained after 200s. The resonance phenomenon is observed with the exited frequency $\omega_e = 1.08rad/s$, in which the steady state amplitude of the displacement at buffer is over 10 times of amplitude of the excited oscillation $A_e = 1$. While the excited frequency is $\omega_e = 1.22rad/s$., the buffer oscillation is depressed that the amplitude of the steady-state response is much less than the amplitude of the excited oscillation $A_e = 1$.

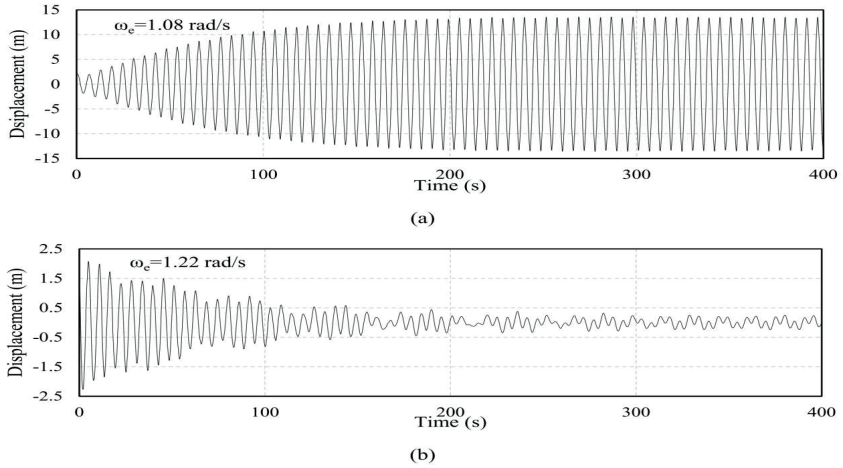

Figure 3 The history of longitudinal displacement at $z = L$ in the reference case. The excited frequency is (a) $\omega_e = 1.08rad/s$ and (b) $\omega_e = 1.22rad/s$

Using the Fast Fourier Transport method, the histories of the longitudinal displacement at $z = L$ are transformed into the frequency domain and depicted in Figure 3(a) for the excited frequencies $\omega_e = 0.2,1.08$ and $1.22\ rad/s$ It shows that the peaks with the maximum amplitudes have the frequency identical to the excited frequencies ω_e This observation indicates that the heave motion predominates the dynamic response of the fluid-filled lifting pipe accounting for the fluid-structural interaction. To determine the

response frequency in the fluid-filled pipe with one-end closed subjected to the heave motion, the dynamic amplification factor for various excited frequency in the range of ω_e~(0,2rad/s] are plotted in Figure 3(b). It shows that the resonance frequencies of the fluid-filled rising pipe are $\omega_e = 0.4,1.08\ and\ 1.62\ rad/s$. The water hammer wave speed accounting for fluid-structural interaction effect has been proposed by Tijsseling (1990) in the form as

$$a_w = \sqrt{\frac{K_f/\rho}{1+\left(1-\nu^2\right)\frac{2K_f R_0}{Eh}}} \tag{4}$$

The water hammer wave accounting for the fluid-structural interaction effects is $a_w = 1296m/s$ with a fundamental frequency of $a_w/4L = 0.407rad/s$. Obviously, the first resonance frequency is due to water hammer wave oscillation. The axial wave speed in the rising pipe wall is identical to the sound wave in the pipe material as $a_s = \sqrt{E/\rho_s} = 5189m/s$ with a fundamental frequency of $a_s/4L = 1.63rad/s$. It's obviously that the third resonance frequency is dominated by the axial stress in the pipe wall. It shows that the third resonance frequency is close to the frequency of the axial wave rather than the frequency for the first mode ($\omega_1 = 1.57rad/s$). In other way, accounting for the fluid-structural interaction, the buffer and pump shift the frequency for the first mode without influence the resonance frequency dominated by the structural dynamic response. The second resonance frequency is close to the average frequency of the first and third resonance frequencies. Physically, the combination of the water hammer wave and the axial stress wave is resonance with the excited frequency.

The first two resonance frequencies can be obtained from the spectrum of the displacement at buffer excited by heave motion with any frequency, as shown in Figure 3(a). Except the peaks dominate by the excited frequencies, Figure 4(a) shows that any peaks or dips in the displace spectrum corresponding to a resonance frequency predicted by the curve of dynamic amplification factor and the excited frequency presented in Figure 4(b). Setting the excited frequency as ω_e=0.2,1.08rad/s, the spectrums of the displacements at the buffer are unable to predict the resonance frequency of ω=1.63rad/s that dominated by axial stress propagation. Hence, in order to predict the resonance frequency from the spectrum of the displacement at buffer subjected to specified excited frequency, one should include the resonant dominated by axial stress propagation. Compared to the method using the spectrum of the displacement, the method obtained the dynamic amplification factor for all excited frequency in the interested range requires more computation efforts. However, it provides more details than the spectrum method, such as the dynamic amplification factor and the frequency for the anti-resonance, e.g., the dynamic amplification factor at ω_e=1.22rad/s that means the buffer oscillation is diminished due to fluid-structural interaction effects.

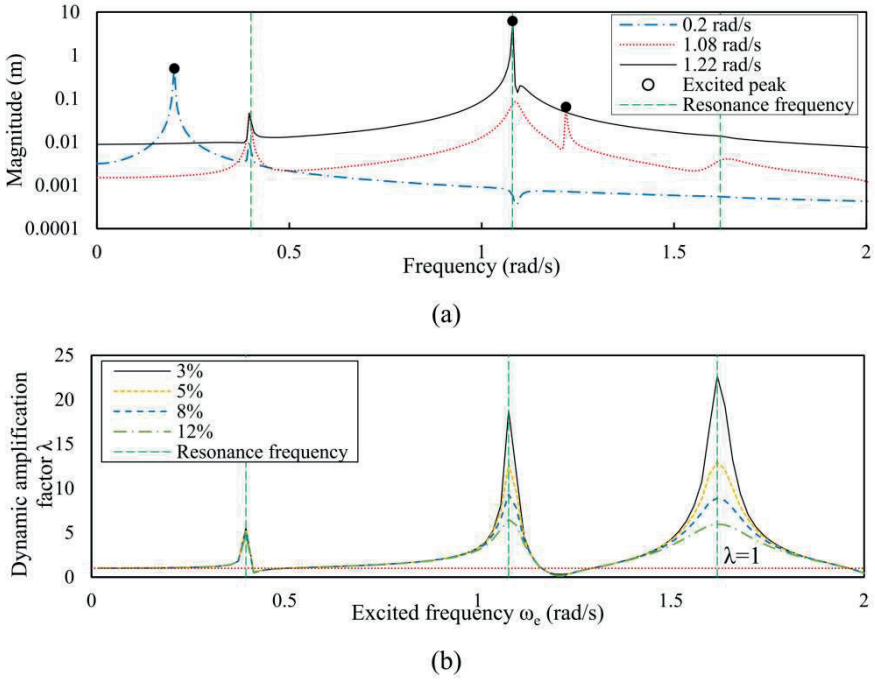

Figure 4 (a)Single-sided amplitude spectrum of the history of displacement at the buffer for three excited frequencies; (b) Dynamic amplification factor using various viscous damping ratio with the excited frequency in the range of $\omega_e \sim [0.02,2] rad/s$.

5.2 EFFECTS OF PIPE LENGTH AND BUFFER MASS ON THE DYNAMIC RESPONSE OF FLUID-FILLED RISING PIPE

Fixing the length of section OP at $L_1 = 200m$ and varying the length L_2 of the section PB, the pipe length $L = L_1 + L_2$ decreases from 5000m to 1000m with an interval of 500m. The excited frequency ω_e increase from 0 rad/s to 2 rad/s with an interval of 0.02 rad/s. The first radial predominate frequency is fixed, and the longitudinal predominate frequency is updated for each run with different pipe length. The Courant number is set as $L/500$. The rest parameters are the same as provided in the reference case. To investigate the difference between the displacement at the buffer to the displacement at the top of the lifting pipe, the dynamic amplification factor is introduced as

$$\lambda = \frac{\sum_{i=1}^{4} A_{b,i}}{\widetilde{A_e}} \tag{5}$$

where $A_{b,i}\ i = 1,2,3$ are the amplitudes of the first four maximum peaks in frequency domain transformed from the history of displacement at the buffer, $\widetilde{A_e}$ is the amplitude of the excited displacement history at the top of the lifting pipe in frequency domain. Since

the simulation time is finite, the amplitude $\widetilde{A_e}$ extracted from the numerical model is slightly difference to A_e used to definite the amplitude of the forced oscillation.

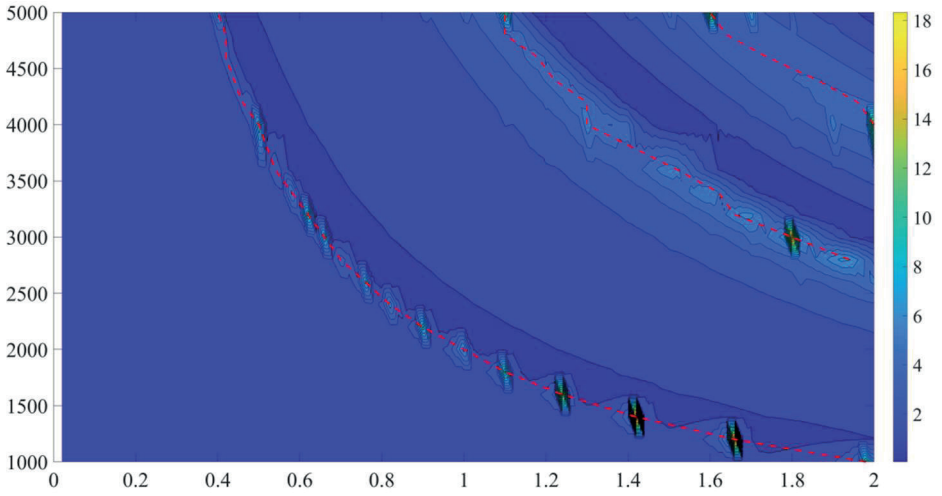

Figure 5 Effect of the pipe length on dynamic response of fluid-filled lifting pipe subjected to various frequency of heave motion

Figure 5 depicts the contours of the dynamic amplification factor λ for different length of the lifting pipe with various excited frequency in the range [0.02,2] rad/s. It shows that three resonance frequencies shift to higher frequency as decrease the length of lifting pipe. As a result, some resonant observed in rising system with $L = 5000m$ is not activated in the investigated frequency range for a shorter rising pipe. The white dash lines in Figure 5 relates the three resonance frequencies to the rising pipe length for three and can be fitted by the following expression

$$\omega_i = \frac{2\pi a_i}{4L} \tag{6}$$

in which $i = 1,2,3$ refers to three peaks observed in Figure 6. The fitting parameters are $a_1 = 1261.14m/s$, $a_2 = 3426.9m/s$ and $a_3 = 5135m/s$ with the coefficient of determination $R^2 \geq 0.99$. The values of a_1 and a_3 are closed to the wave speed of the classical water hammer wave speed $a_w = 1296m/s$ and the longitudinal stress wave speed $a_s = 5189m/s$. This observation indicates that the first and third resonance frequencies are dominated by propagation of the water hammer wave and the longitudinal stress wave, respectively. The value of a_2 is closed to the mean values of a_1 and a_2. Hence, the second resonant phenomenon is the results from the coupling effects between the water hammer wave and the longitudinal stress wave.

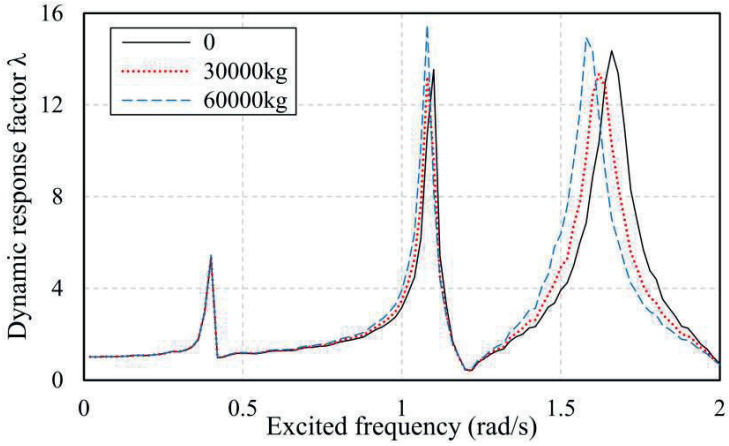

Figure 6 Effects of the buffer mass on the rising pipe dynamic response

Figure 6 depicts the relation of the dynamic response factor λ and the excited frequency with various buffer mass. It shows that the buffer mass has negligible effect on the first resonance frequency $\omega_1 = 0.4rad/s$ which is dominated by the water hammer wave speed. Increase of the buffer mass decreases the second ($\omega_2 \approx 0.4rad/s$) and third ($\omega_3 \approx 1.62rad/s$) resonance frequencies. This observation is consistent to the mass effects on the frequency shifting in the empty pipe.

5.3 EFFECTS OF THE FLUID INITIAL VELOCITY ON THE DYNAMIC RESPONSE OF THE FLUID-FILLED LIFTING PIPE

The initial fluid velocity is varied in the reference case to investigate its effect on the dynamic response of the rising pipe subjected to sinusoidal heave motion. Since the dynamic response of the rising pipe is dominated by the heave motion, Figure 7(a) shows that the initial fluid velocity has negligible influence on the dynamic response of the rising pipe. Due to the resonant, the amplitude of the peak in the displacement spectrum at $w = 0.4rad/s$ with the excited frequency $w_e = 0.4rad/s$ is much higher than those with other excited frequency, which is removed from plotted in Figure 7(b). It shows that the amplitudes for the peak in the displacement spectrum at $w = 0.4rad/s$ are proportional to the magnitude of the initial fluid velocity. The direction of the initial fluid velocity has negligible effects on the dynamic response of the rising pipe with one-end closed while subject to sinusoidal heave motion.

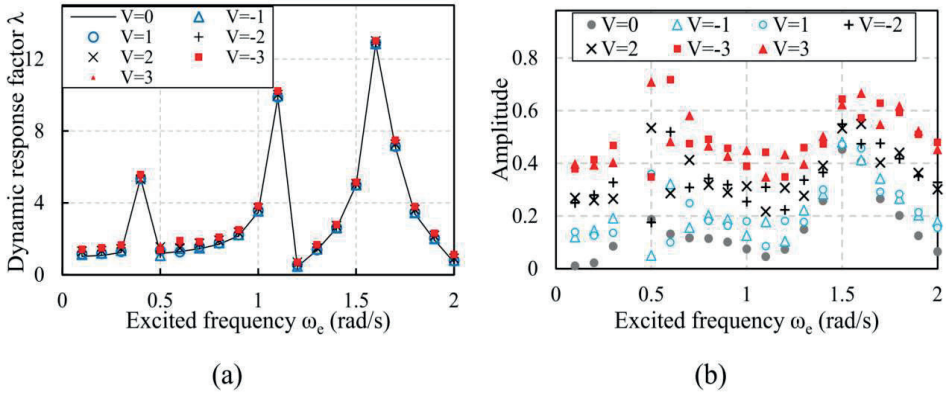

Figure 7 Effects of the fluid initial velocity on the rising pipe dynamic response

6. CONCLUSIONS

Subjected to sinusoidal heave motion, the dynamic response of the lifting pipe system is solved using the finite element using the partitioned shell-based water hammer model. The effects of the masses of intermediate pump and buffer at the bottom of the pipe, as well as the length of the lifting pipe, have been investigated for the dynamic response of lifting pipe. In additional, the effect of the initial flow velocity has been investigated for dynamic response of the fluid-filled pipe subjected to sinusoidal heave motion. For conveniently comparation, the time domains of displacement histories are transformed into frequency domain using the Fast Fourier Transform method. The dynamic amplification factor is introduced to illustrate the difference between the dynamic response at the bottom of the lifting pipe and the forced oscillation top of the pipe. The following conclusions and observations can be drawn from the investigated problem in the present study:

(1) The frequencies of the dynamic responses at the bottom of a fluid-filled lifting pipe are predominated by the excited frequency of the heave motion.

(2) From the response spectrum for the dynamic response at the bottom of the fluid-filled pipe, one can extract the frequencies for the first two resonances that correspond to the water hammer pressure wave and the coupling between the pressure wave and stress wave in the pipe. Hence, the natural frequency for the empty pipe should be conducted to extract the resonance frequency corresponding to the longitudinal vibration of the lifting pipe.

(3) There is always an excited frequency a bit over than the resonance frequency to depress the dynamic response of the lifting pipe. This characteristic can be used for the control of longitudinal vibration.

REFERENCES

1. Bai, Y., Xie, W., Gao, X., & Xu, W. ,2018. Dynamic analysis of a cantilevered pipe conveying fluid with density variation. Journal of Fluids and Structures, 81, 638–655.
2. Budny, D. D., Wiggert, D. C., & Hatfield, F., 1990. Energy Dissipation in the axially-coupled model for transient flow. In A. R. D. Thorley (Ed.), Proceedings of the 6th International

Conference on Pressure Surges (pp. 15–26). BHRA.
3. Budny, D. D., Wiggert, D. C., & Hatfield, F. J.,1991. The Influence of Structural Damping on Internal Pressure During a Transient Pipe Flow. Journal of Fluids Engineering, 113(3), 424–429.
4. Cao, H., Mohareb, M., & Nistor, I., 2020. Finite element for the dynamic analysis of pipes subjected to water hammer. Journal of Fluids and Structures, 93, 102845.
5. Cao, H., Mohareb, M., & Nistor, I., 2021. Partitioned water hammer modeling using the block Gauss–Seidel algorithm. Journal of Fluids and Structures, 103, 103260.
6. Chatjigeorgiou, I. K., 2010. On the effect of internal flow on vibrating catenary risers in three dimensions. Engineering Structures, 32(10), 3313–3329.
7. Daude, F., & Galon, P., 2018. A Finite-Volume approach for compressible single- and two-phase flows in flexible pipelines with fluid-structure interaction. Journal of Computational Physics, 362, 375–408.
8. Gale, J., & Tiselj, I., 2008. Godunov's Method for Simulatinons of Fluid-Structure Interaction in Piping Systems. Journal of Pressure Vessel Technology, 130(3).
9. Ghidaoui, M. S., Zhao, M., McInnis, D. A., & Axworthy, D. H., 2005. A review of water hammer theory and practice. Applied Mechanics Reviews, 58(1), 49.
10. Giacobbi, D. B., Rinaldi, S., Semler, C., & Païdoussis, M. P., 2012. The dynamics of a cantilevered pipe aspirating fluid studied by experimental, numerical and analytical methods. Journal of Fluids and Structures, 30, 73–96.
11. Heffernan, O., 2019. Deep-sea dilemma:Mining the ocean floor could solve mineral shortages-and lead to epic extinctions in some of the most remote ecosystems on Earth. Nature, 465–469.
12. Kuiper, G. L., & Metrikine, A. V.,2005. Dynamic stability of a submerged, free-hanging riser conveying fluid. Journal of Sound and Vibration, 280(3), 1051–1065.
13. Kuiper, G. L., & Metrikine, A. V., 2008. Experimental investigation of dynamic stability of a cantilever pipe aspirating fluid. Journal of Fluids and Structures, 24(4), 541–558.
14. Lavooij, C. S. W., & Tijsseling, A. S., 1991. Fluid-structure interaction in liquid-filled piping systems. Journal of Fluids and Structures, 5(5), 573–595.
15. Paidoussis, M. P., 1970. Dynamics of Tubular Cantilevers Conveying Fluid. Journal of Mechanical Engineering Science, 12(2), 85–103.
16. Paidoussis, M. P., 1999. Aspirating pipes do not flutter at infinitesimally small flow. Journal of Fluids and Structures, 13(3), 419–425.
17. Paidoussis, M. P., & Luu, T. P., 1985. Dynamics of a Pipe Aspirating Fluid Such as Might be Used in Ocean Mining. Journal of Energy Resources Technology, 107(2), 250–255.
18. Skalak, R., 1953. An extension of the theory of water hammer. Columbia University.
19. Sparenberg, O., 2019. A historical perspective on deep-sea mining for manganese nodules, 1965–2019. The Extractive Industries and Society, 6(3), 842–854.
20. Tijsseling, A. S., 1996. Fluid-structure interaction in liquid-filled pipe system: a review. Journal of Fluids and Structures, 10(2), 109–146.
21. Tijsseling, A. S., Lambert, M. F., Simpson, A. R., Stephens, M. L., Vítkovský, J. P., & Bergant, A., 2008. Skalak's extended theory of water hammer. Journal of Sound and Vibration, 310(3), 718–728.
22. Tijsseling, A. S., & Lavooij, C. S. W., 1990. Waterhammer with fluid-structure interaction. Applied Scientific Research, 47(3), 273–285.
23. Tijsseling, A. S., & Vaugrante, P., 2001. FSI in L-shaped and T-shapred pipe systems. 10th Internation Meeting of Work Group on the Behavior of Hydraulic Machinery under Steady Oscillatory Conditions.
24. Vardy, A. E., Fan, D., & Tijsseling, A. S., 1996. Fluid-structure interaction in a T-piece pipe. Journal of Fluids and Structures, 10(7), 763–786.
25. Verichev, S., Metrikine, A., Plat, R., & Hendrikse, H., 2011. Dynamics of the Vertical Hydraulic Transport System for Deep Sea Mining (pp. 461–468).

26. Wiggert, D. C., & Sundquist, M. J., 1997. Transients, fixed-grid characteristics for pipeline. Journal of the Hydraulics Division, 103(12), 1403–1416.
27. Wiggert, D. C., & Tijsseling, A. S., 2001. Fluid transients and fluid-structure interaction in flexible liquid-filled piping. Applied Mechanics Reviews, 54(5), 455–481.
28. Williams, D. J., 1977. Waterhammer in non-rigid pipes: precursor waves and mechanical damping. Journal of Mechanical Engineering Science, 19(6), 237–242.